Longitudinal-phase-space analysis of $\pi^+ n \to \pi^+ \pi^- p$ at 15 GeV/c*

J. E. Richey,† V. Hagopian, J. D. Kimel, S. Hagopian, J. E. Lannutti, B. Wind, C. P. Horne,‡ and N. D. Pewitt§
Florida State University, Tallahassee, Florida 32306

J. R. Bensinger
Brandeis University, Waltham, Massachusetts 02154

H. O. Cohn
Oak Ridge National Laboratory, Oak Ridge, Tennessee 37830
(Received 30 November 1976)

3114 events of the reaction $\pi^+ d \to \pi^+ \pi^- p p_s$, where p_s is a nonparticipating spectator, were studied in the SLAC 82-inch bubble chamber. A longitudinal-phase-space (LPS) analysis was performed to separate the various t-channel exchange mechanisms, e.g., π or Pomeron exchange. The validity of the LPS method was tested for pion exchange by generating events using the one-pion-exchange model modified by absorption (OPEA). The model and the data agreed extremely well. The principal features of the data include the ρ^0, f^0, Δ^0, and N^*'s. The LPS analysis also reveals the g^0, but a slight modification of the standard LPS selection criteria enhances the g^0, as expected by OPEA-model calculations.

I. INTRODUCTION

The $\pi\pi$ scattering amplitudes for dipion masses below 2 GeV have been studied extensively. The usual technique of extracting the $\pi\pi$ phase shifts is the method of using the one-pion-exchange (OPE) model and extrapolating the data to the pion pole.[1-6] In addition, major theoretical work has been done in understanding the data in the physical region by modifying OPE models with absorption (OPEA). Most of the information on $\pi\pi$ phase shifts comes from the reactions $\pi^- p \to \pi^- \pi^+ n$ and $\pi^+ p \to \pi^+ \pi^- \Delta^{++}$. In general only a part of the data from these reactions corresponds to one-pion exchange, while the rest are explained by other diagrams such as Pomeron, ρ, or N exchanges.

The data of this experiment on $\pi^+ n \to \pi^+ \pi^- p$ are no exception and about one-half of the events correspond to OPE. In order to separate the OPE part from the rest of the events a longitudinal-phase-space (LPS) analysis was performed. To test the validity of this analysis the Monte Carlo technique was used to generate events using the OPEA as developed in the theoretical work of several physicists.[7-9] The result is that the LPS selection criteria of positive longitudinal momentum for both π^+ and π^- do indeed choose the one-pion-exchange events with prominent ρ^0 and f^0. Owing to kinematical constraints the LPS cut also removes the very forward and very backward π^+'s of f and g events (in the helicity frame). A small modification of the standard LPS brings in most of the g events although, unfortunately, together with some non-OPE background.

Section II reviews briefly the experimental details. Section III presents the general features of the reaction $\pi^+ d \to \pi^+ \pi^- p p_s$ at 15 GeV/c. Section IV describes a one-pion-exchange model modified by absorption (OPEA) and Sec. V applies this model to the data. The inputs to this model are the known π-π phase shifts[6] (δ_0^0, δ_1^1, δ_2^0, δ_3^1) with all model parameters being determined from data other than from this experiment. New to this work is the application of a full Monte Carlo treatment of the OPEA contribution to this reaction. This approach makes possible the calculation of several distributions inaccessible to the usual analytic treatment of OPEA. Section VI summarizes the conclusions.

II. EXPERIMENTAL METHOD

The data presented here are from an exposure of 890 000 pictures in the SLAC deuterium-filled 82-in bubble chamber. The 15 GeV/c rf-separated beam was ~97% π^+, with ~3% μ^+ contamination. The first set of data consisting of 370 000 pictures was measured on the University of Pennsylvania Hough-Powell device (HPD), operated in the minimum-guidance mode, using an automatic track-following program. The second set of 520 000 pictures was measured at the Oak Ridge National Laboratory on the University of Tennessee spiral reader.

The scanning criteria selected three- and four-prong events. Three-prong events were required to have one dark track, which was required to have a curvature corresponding to a momentum of less than 650 MeV/c, or stop in the chamber. The four prongs were required to have at least one stopping dark track.

The reconstruction and kinematics programs employed were TVGP and SQUAW. Each event in the first set of data was sent to an experienced scanner to check the predicted bubble density with the bubble density on film for particle identification. For the second set, the spiral-reader pulse-height information was compared to TVGP predicted bubble density. Only 16% of the events in this second set had to be manually checked for bubble-density information.

Events were further required to have a χ^2 probability of greater than 0.1%, be at least a three-constraint fit, and have missing mass squared between −0.12 and 0.12 GeV^2. This resulted in a final sample of 3114 events, corresponding to a cross section of 376 ± 25 μb.[10]

III. GENERAL FEATURES OF THE FINAL STATE $\pi^+ n \to \pi^+\pi^- p$

The $\pi^+\pi^-$ invariant-mass spectrum for events fitting $\pi^+ d \to \pi^+\pi^- p p_s$, where p_s is the nonparticipating spectator proton, is shown in Fig. 1. Clear ρ^0 and f^0 meson production is seen; however, no g signal can be discerned in this plot. The $\pi\pi$ mass resolution up to 2 GeV is approximately 20 MeV. The $p\pi^+$ and $p\pi^-$ mass spectra are shown in Fig. 2. The $p\pi^+$ distribution shows a broad high-mass enhancement while the $p\pi^-$ system shows a broad low-mass enhancement. Examination of the corresponding Dalitz plots (not shown) showed most of the low-mass enhancement in the $p\pi^-$ events to be Δ and N^*'s which correspond to target dissociation, with the rest reflections of ρ, f, and g and all the events in the broad high-mass peak of $p\pi^+$ to be reflections of Δ, N^*, ρ, and f resonances.

In this experiment the three main exchange processes for the reaction $\pi^+ n \to \pi^+\pi^- p$ are pion exchange, A_2 exchange, and Pomeron exchange. The longitudinal-phase-space technique as developed by Van Hove[11] was utilized to help separate these contributions. This method takes advantage of the well-known fact that the momentum transverse to the beam direction is small in high-energy hadron collisions, peaking at about 300 MeV/c. This fact allows the clear separation of phase space into longitudinal and transverse parts, so that for an n-particle final state the longitudinal-phase-space distribution reduces to a manifold of $n-2$ dimensions (i.e., one dimension for this reaction). This reduction in the dimension of particle phase space simplifies the separation of competing exchange mechanisms. Figure 3(a) shows schematically an event plotted in terms of two variables (r, ω), where ω is the Van Hove angle and r is defined below. In this scheme the longitudinal momentum q in the $\pi^+ n$ center-of-mass system of each outgoing particle can be written as

$$q_1 = q_p = -r\sin\omega\,,$$

$$q_2 = q_{\pi^+} = -r\left(\frac{\sqrt{3}}{2}\cos\omega - \tfrac{1}{2}\sin\omega\right),$$

$$q_3 = q_{\pi^-} = r\left(\frac{\sqrt{3}}{2}\cos\omega + \tfrac{1}{2}\sin\omega\right),$$

so that

$$r = (2/3)^{1/2}(q_{\pi^-}{}^2 + q_{\pi^+}{}^2 + q_p{}^2)^{1/2}.$$

Figure 3(b) shows the distribution of events in the longitudinal-phase-space plot. Since the transverse momentum is not zero, but is distributed about zero, the events deviate from the polyhedral boundary. Some deviation is also due to the fact that in deuterium experiments the c.m. energy is not constant. The net result of these two factors

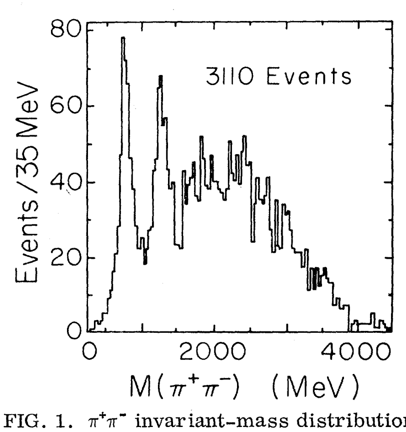

FIG. 1. $\pi^+\pi^-$ invariant-mass distribution.

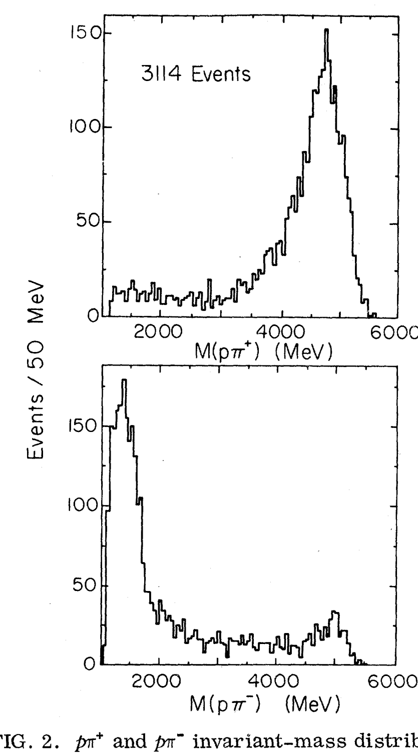

FIG. 2. $p\pi^+$ and $p\pi^-$ invariant-mass distributions.

is a rounding off of the vertices and a loss of definition of the sides of the polyhedral boundaries as seen in Fig. 3(b).

Figure 3(b) contains six sectors where the majority of each sector's events can be represented by its most likely exchange mechanism, as shown in Fig. 4. Since the proton is backward in the center-of-mass system for over 98% of the events it is clear that the reaction is dominated by π and A_2 exchange and Pomeron exchange (sectors 2 and 3, respectively).

The fraction of events is 42% for sector 2 (pion exchange, A_2 exchange); 50% in sector 3 (Pomeron exchange); 4%in sector 1. The sector-1 events will be discussed in detail in the following section. It is worthwhile pointing out the 15 events ($\sigma = 4.7$ μb) clearly separated in sector 5 corresponding to nucleon exchange.

The selection criterion of the three-prong events is that the proton momentum be less than 650 MeV/c. This selection removes about $\frac{2}{3}$ of the events in sectors 4 to 6 and less than 10% of the events in

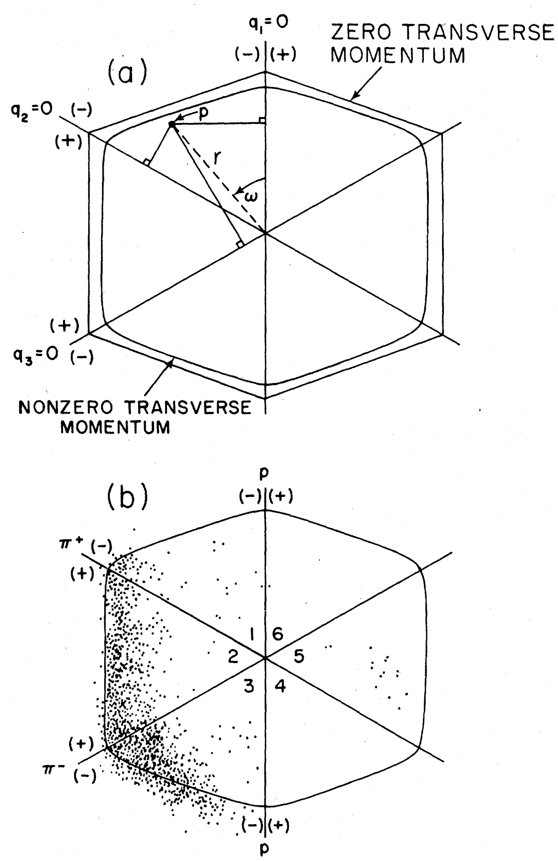

FIG. 3. (a) Van Hove diagram for $n=3$ showing one point $P(q_1, q_2, q_3)$ and the definition of the Van Hove angle ω and radius r; (b) Van Hove plot of the longitudinal-phase-space distribution for the $\pi^+n \to \pi^+\pi^-p$ events.

sectors 1 to 3. Since the one-pion-exchange contribution is dominant for small t [$|t| < 0.2$ (GeV/$c)^2$], this selection criterion does not effect our analysis of OPE.

IV. ONE-PION-EXCHANGE MODEL WITH ABSORPTION

A one-pion-exchange model with absorption as developed by Kimel and Reya[7] was employed to generate events via a Monte Carlo technique.

The model

In the s-channel helicity frame, the differential cross section is given by[7]

$$\frac{d^3\sigma}{dt\,ds'\,d\Omega} = \frac{\tilde{p}}{2\pi p^2 s\sqrt{s'}} \sum_{\lambda,\mu} |M_{\lambda\mu}|^2. \tag{1}$$

where s is the c.m. energy squared, t is the square of the four-momentum transferred between the nucleons, s' is the square of the $\pi\pi$ effective mass, p is the initial state c.m. momentum, $\tilde{p}$ is the momentum of the final-state pions in the dipion rest frame, and $d\Omega$ denotes the decay direction of the final state π^+. The one-pion-exchange (OPE) amplitudes, with appropriate modifications due to absorption, are known[4,7] to dominate the charge-symmetric reaction $\pi^-p \to \pi^-\pi^+n$ (for small $|t|$), and have been successfully used in that reaction to obtain dependable $\pi\pi$ phase shifts[6] over an impressive range of $\pi\pi$ energies. This development makes possible the construction of a parameter-free OPE model to compare with our data.

The OPE amplitudes can be expanded in terms of the on-shell $\pi\pi$ phase shifts as

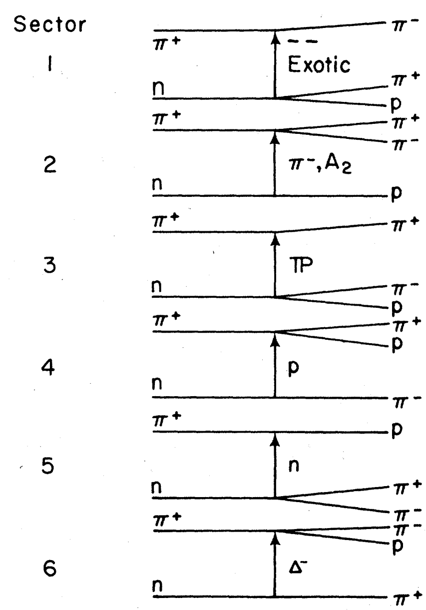

FIG. 4. Correspondence between LPS sectors and most likely exchange mechanisms for the reaction $\pi^+n \to \pi^+\pi^-p$.

$$M_{\lambda\mu}=\frac{G\sqrt{s'}}{\sqrt{4\pi}\,\tilde{p}}\sum_{l,m,I}(2l+1)C_I e^{i\delta_l^I}\sin\delta_l^I \times B^l_{m\lambda\mu}d^l_{m0}(\theta)e^{im\phi}, \tag{2}$$

where the C_I are the usual isospin factors, G is the π-N coupling constant ($G^2/4\pi=14.4$), $\mu(\lambda)$ is the helicity of the initial-state (final-state) nucleon, and d^l_{m0} are the rotation functions. The amplitude $B^l_{m\lambda\mu}$ describes the production, due to pion exchange, of an intermediate dipion system of spin l, mass $\sqrt{s'}$, and helicity m. Because $t_{\min}$, the kinematic limit of the four-momentum transfer squared, can be neglected at our energy, the dominant amplitudes have nucleon helicity flip and are given by

$$B^l_{m+-}=\frac{(-t)^{n/2}P^l_{m+-}(t)}{m_\pi^{\,2}-t}, \tag{3}$$

in which n is the net helicity flip and $P^l_{m+-}(t)$ are the polynomials in t documented in Ref. 7.

The effects of absorption can be taken into account by replacing (3) with

$$B^{l\,\mathrm{abs}}_{m+-}=\frac{(-t)^{n/2}P^l_{m+-}(m_\pi^{\,2})}{m_\pi^{\,2}-t}F_n(t), \tag{4}$$

where $F_n(t)$ is an absorption-induced collimating factor. Other studies have shown[7,9] that, except for $n=0$, the collimating factors exhibit only a weak dependence on the net helicity flip and so $F_n(t)=F_1(t)$ was set for $n\neq 0$. On the other hand, $F_0(t)$ has an additional, approximately linear, dependence on t:

$$F_0(t)=F_1(t)[1+\mathcal{A}_0(t-m_\pi^{\,2})]. \tag{5}$$

The parameter $\mathcal{A}_0(s')$ reflects the stronger effects of absorption in the $n=0$ amplitude. Finally, in the small-$|t|$ region, the collimating factor $F_1(t)$ can be well represented by an exponential form $\exp[b(t-m_\pi^{\,2})]$. With these approximations our formulation of the absorption model of Kimel and Reya is identical to the generalization of the Williams model[8] proposed by Estabrooks *et al.*[9] The relation between $\mathcal{A}_0$ and C, the effective cut parameter introduced by the latter authors, is $\mathcal{A}_0=(1-C)/m_\pi^{\,2}$. The absorption parameters are listed in Table I.

As established in previous analyses,[9] the slope b, shown in Table I, is taken as constant over the dipion masses considered here. However, it has been suggested that the effective cut strength C falls with increasing $\pi\pi$ mass, being considerably smaller for the f and g than for the ρ.[9] We have roughly included this dependence in our calculation by using for each resonant production amplitude a different (but constant) effective C evaluated at the corresponding resonance mass, as shown in Table I.

TABLE I. Resonance parameters for OPEA model.

	M (MeV)	Γ (MeV)	X	R (GeV)$^{-1}$	b (GeV/c)$^{-2}$	C
ρ	778	152	1.0	4.5	5	0.85
f	1279	202	0.84	5.3	5	0.5
g	1713	228	0.26	6.4	5	0.5

With the specification of the on-shell $\pi\pi$ partial-wave scattering amplitudes, the OPE absorption model is completely determined. The dominant contributions to the $\pi\pi$ amplitude come from the δ_1^1, δ_2^0, and δ_3^1 phase shifts manifested in the ρ, f, and g resonances, respectively. These phase shifts have been measured by the CERN-Munich group from an analysis[6] of the high-statistics experiment on $\pi^-p\to\pi^+\pi^-n$ at 17.2 GeV/c. It is convenient here to use the Breit-Wigner parametrization determined in Ref. 6 for δ_1^1, δ_2^0, and δ_3^1:

$$e^{i\delta_l^I}\sin\delta_l^I=\frac{X_l^I(s_{0l}^I)^{1/2}\Gamma_l^I}{s_{0l}^I-s'-i(s_{0l}^I)^{1/2}\Gamma_l^I}, \tag{6}$$

where $(s_{0l}^I)^{1/2}$ is the resonance mass, X_l^I is the elasticity, and the energy-dependent width Γ_l^I is taken to be

$$\Gamma_l^I=\Gamma_{0l}^I\left(\frac{\tilde{p}}{\tilde{p}_0}\right)^{2l+1}\frac{D_l(\tilde{p}_0R)}{D_l(\tilde{p}R)}. \tag{7}$$

Here R is the range, $\tilde{p}_0$ is the momentum of a final-state pion at the resonance mass, and the D_l's have been parametrized in the standard form.[12] The resonance parameters measured in Ref. 6 are given in Table I. For the isoscalar s-wave $\pi\pi$ amplitude, not representable as a simple Breit-Wigner, the δ_0^0 phase shifts of Ref. 6 were used directly by fitting them to a polynomial in dipion mass, a form convenient for the Monte Carlo calculations. The small contribution of the isotensor s wave is neglected.

V. COMPARISON OF THE MODEL TO THE DATA

The one-pion-exchange model with absorption (OPEA) is compared to the experimental data on the basis of the LPS analysis. LPS is used to separate out the events that correspond as closely as possible to one-pion exchange. Excellent agreement between the model and the data are obtained by this method.

A plot of LPS for events generated by the model is shown in Fig. 5. From this distribution it is clear that just selecting data in LPS sector 2 will not isolate the OPE, since 12% of the model data lie in sector 3, and 9% in sector 1. As a result of this, a new selection criterion was defined. This consisted of defining the LPS region which corresponds to OPE to be $55° \leq \omega \leq 125°$, where ω is the Van Hove angle as defined in Fig. 3(a). The correlation of $\pi\pi$ mass versus ω is shown in Fig. 6. The data are shown in Fig. 6(a) while the model events are shown in Fig. 6(b). It is clear that a cut in ω between 60° to 120° does not remove any ρ events while it does remove a few f events and more g events. A cut in ω of 55° to 125° leaves the model events mostly intact. The non-OPE events are seen in Fig. 6(a) at high $\pi\pi$ mass and near maximum kinematically possible ω. The 55° to 125° cut lets in some of these non-OPE events.

Events with A_2 exchange can also populate sector 2. However, A_2 exchange does not become dominant until $|t|$ is typically greater than 0.2 (GeV/$c)^2$.[13] It has also been shown that the exchange of an A_2 Regge pole with $|t| < 0.1$ (GeV/$c)^2$ accounts for less than 5% of the integrated ρ cross section in this energy region[13] and that the OPEA parametrization used here should be adequate to describe the data for small t.[14]

On the basis of the preceding discussion, a new cut on the Van Hove angle is defined such that ω lies in the interval from 55° to 125° and $|t| \leq 0.2$ (GeV/$c)^2$ (from now on referred to as the VHWT cut), to be contrasted with the cut [LPS sector 2 and $|t| < 0.2$ (GeV/$c)^2$], referred to as the LPST cut. Detailed comparison can now be made of the relevant kinematical quantities of invariant masses, t distributions, angular distributions, and longitudinal and transverse momenta of each outgoing particle of the OPEA model to the real data.

In Fig. 7 the longitudinal and transverse momentum distributions are shown after an LPST cut. As is well known, the transverse momentum of all outgoing particles is small, peaking at about 300 MeV/c. In contrast, the longitudinal momentum of the outgoing particles is distributed very differently. The OPEA model is successful in reproducing all of the major features of these distributions as shown by the smooth curves. No statistically significant difference is discernable in the longitudinal- and transverse-momentum distributions after the VHWT cut (not shown).

The dipion-invariant-mass distributions for the LPST and VHWT cuts are shown in Fig. 8. In both plots the OPEA curves are normalized to events in the interval 280 to 1600 MeV. This normalization was chosen because it avoids the problem that events with high dipion mass and hence large momentum in the dipion rest frame overlap into sectors 1 and 3. The two plots agree almost exactly in the mass region 280 to 1000 MeV. Above 1000 MeV the VHWT cut brings out the f and especially the g signal, even though above 1500 MeV some non-OPE background is also present.

The OPEA gives excellent agreement for the s-channel helicity angular distributions. The s-channel helicity angle $\cos\theta$ is defined in the $\pi^+\pi^-$ center-of-mass system as

$$\cos\theta = \frac{-\vec{p}_2 \cdot \vec{p}_3}{|\vec{p}_2||\vec{p}_3|},$$

in which $\vec{p}_2$ is the proton momentum and $\vec{p}_3$ is the final-state π^+ momentum. The helicity distributions for the VHWT cut are shown in Fig. 9 for the three mass regions corresponding to the ρ, f,

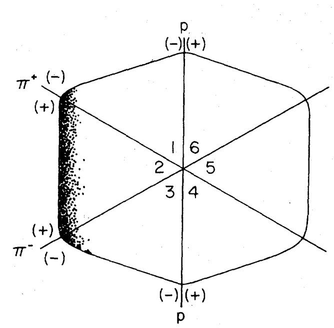

FIG. 5. Longitudinal-phase-space distribution for the Monte Carlo–generated model events for the reaction $\pi^+ n \to \pi^+\pi^- p$.

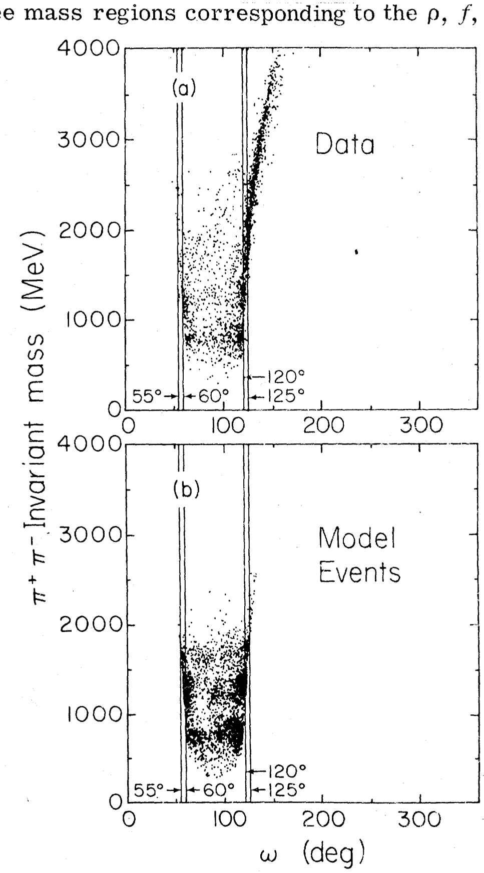

FIG. 6. $\pi^+\pi^-$ invariant mass versus Van Hove angle ω for (a) the data and (b) the model-generated events.

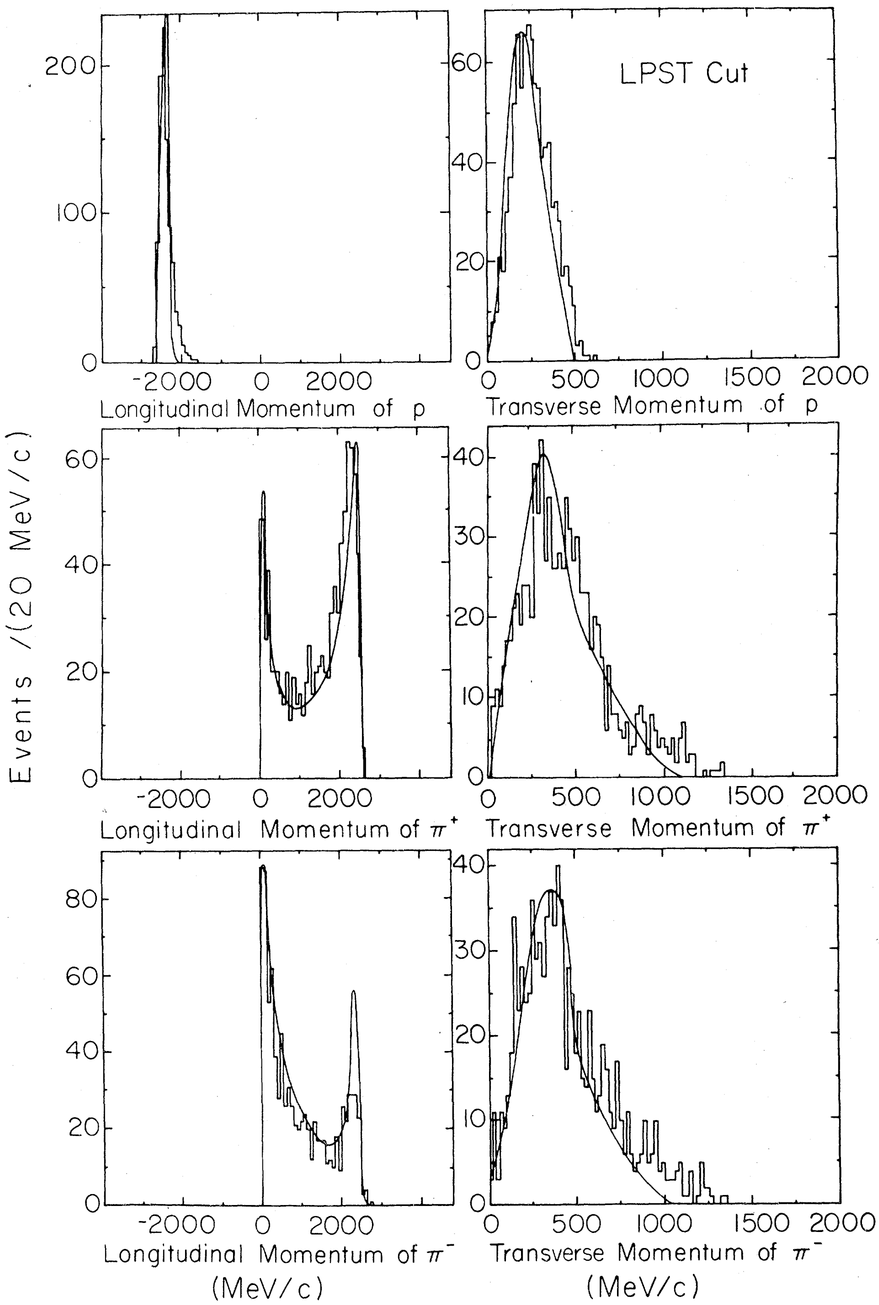

FIG. 7. Longitudinal- and transverse-momentum distributions after the LPST cut. The curves are the OPEA predictions.

TABLE II. Resonance cross sections in reaction $\pi^+d \to p_s pR$ with momentum of $p_s < 300$ MeV/c and $|t| < 0.4$ (GeV/c)^2.

R	Cross section (μb)
ρ	39 ± 4
f	40 ± 4
g	15 ± 5

and g mesons. Again, good agreement is obtained indicating a clean isolation of OPE. Table II lists the cross section of ρ, f, and g with spectator proton momentum < 300 MeV/c and $|t| < 0.4$ (GeV/c)^2.

VI. CONCLUSIONS

The use of longitudinal momentum separates the OPE contribution to the $\pi N \to \pi\pi N$ reaction much

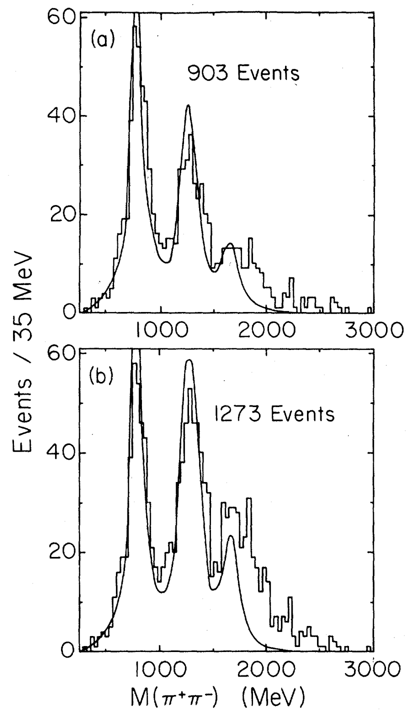

FIG. 8. $\pi^+\pi^-$ invariant mass for (a) LPST cut, and (b) VHWT cut. The OPEA curves are normalized to the interval 280 to 1600 MeV.

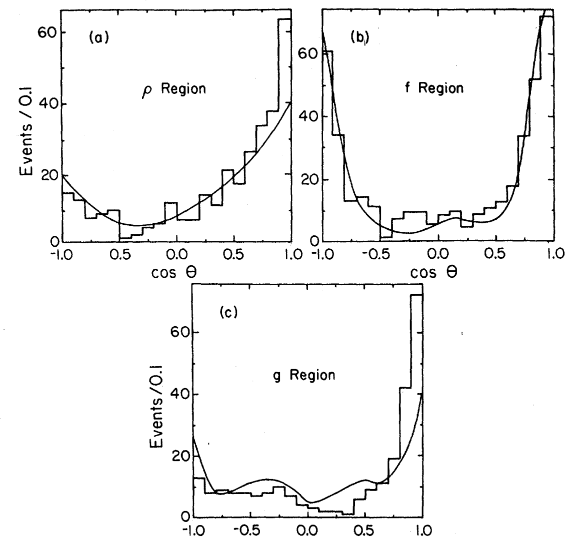

FIG. 9. Events versus cos of the s-channel helicity angle after the VHWT cut for: (a) ρ (650 to 990 MeV); (b) f (1140 to 1380 MeV); (c) g (1500 to 1920 MeV). The curves are the OPEA prediction normalized to the number of events in each plot.

better than the traditional selection methods using small values of t only. In addition, expanding the Van Hove angle cut for OPE from 60°–120° to 55°–125° brings in the high-mass π-π states, such as the g resonance, together with a small amount of non-OPE background. Van Hove-angle cuts should be used with caution since they are correlated with π-π scattering angles. In higher-momentum experiments the LPS method should work well even for higher π-π masses. Most of the events in sector 3 are N^*'s and Δ produced by Pomeron exchange. There is no evidence of any $\Delta^{++} \to p\pi^+$ production.

ACKNOWLEDGMENTS

The authors would like to acknowledge the following persons: Professor P. K. Williams and Professor J. Albright for various discussions; and the staff of the SLAC 82-in. bubble chamber, especially R. Watt and Dr. J. Ballam. We would also like to thank the scanning staff of Florida State University and the measuring staffs of the University of Pennsylvania HPD and the University of Tennessee spiral reader. Special thanks to Professor W. Bugg, Professor G. Condo, and Professor E. Hart of University of Tennessee for enabling us to use the spiral reader and Professor Walter Selove of the University of Pennsylvania for our use of the HPD.

---

*Work supported in part by the U.S. Energy Research and Development Administration.

†Presently at Computer Science Corporation.

‡Presently at Particle Data Group, Lawrence Berkeley Laboratory.

§Presently at Office of Management and Budget, Washington, D. C.

[1]A. Engler *et al.*, Phys. Rev. D 10, 2070 (1974); P. Estabrooks and A. D. Martin, Nucl. Phys. B95, 322 (1975).

[2]J. P. Prukop *et al.*, Phys. Rev. D 10, 2055 (1974).

[3]J. P. Baton, G. Laurens, and J. Reignier, Phys. Lett. 33B, 528 (1970).

[4]P. Baillon *et al.*, Phys. Lett. 35B, 453 (1971).

[5]S. D. Protopopescu *et al.*, Phys. Rev. D 7, 1279 (1973).

[6]B. Hyams *et al.*, in *π-π Scattering—1973*, proceedings of the International Conference, Tallahassee, edited by P. K. Williams and V. Hagopian (American Institute of Physics, New York, 1973), p. 206.

[7]J. D. Kimel and E. Reya, Nucl. Phys. B47, 589 (1972).

[8]P. K. Williams, Phys. Rev. D 1, 1312 (1970).

[9]P. Estabrooks *et al.*, in *π-π Scattering—1973*, proceedings of the International Conference, Tallahassee, edited by P. K. Williams and V. Hagopian (see Ref. 6), p. 37.

[10]More details can be found in J. Richey, Ph. D. disser-

tation, Florida State University, Report No. HEP-76-6-18, 1976 (unpublished).
[11]L. Van Hove, Nucl. Phys. B9, 331 (1969).
[12]J. M. Blatt and V. F. Weisskopf, *Theoretical Nuclear Physics* (Wiley, New York, 1952), p. 213.
[13]J. D. Kimel and E. Reya, Nucl. Phys. B58, 513 (1973).
[14]J. D. Kimel and E. Reya, Phys. Lett. 42B, 249 (1972).